PCCP

RSC Publishing

PAPER

Structural and up-conversion properties of Er^{3+} and Yb^{3+} co-doped $Y_2Ti_2O_7$ phosphors†

Cite this: *Phys. Chem. Chem. Phys.*, 2013, **15**, 3480

B. P. Singh,[a] A. K. Parchur,*[b] R. K. Singh,[a] A. A. Ansari,[c] P. Singh*[a] and S. B. Rai*[b]

Received 23rd November 2012,
Accepted 2nd January 2013

DOI: 10.1039/c2cp44195k

www.rsc.org/pccp

$Y_2Ti_2O_7$ (YTO) and Er^{3+}/Yb^{3+} co-doped $Y_2Ti_2O_7$ (EYYTO) phosphors have been prepared by solid-state reaction method. Structures of YTO and EYYTO phosphors are identified as face centered cubic pyrochlores. Up-conversion emission spectra of EYYTO under 976 nm excitation is studied, which revealed three prominent emission lines at ~524, 548 and 661 nm originating from $^2H_{11/2} \rightarrow {}^4I_{15/2}$, $^4S_{3/2} \rightarrow {}^4I_{15/2}$ and $^4F_{9/2} \rightarrow {}^4I_{15/2}$ electronic transitions of Er^{3+} ion, respectively in green and red regions. The power dependence study suggests that these bands arise due to two photon absorption. The monodispersed laser ablated colloidal solution of EYYTO shows strong red and green emissions on excitation with 976 nm laser. The variation of luminescence intensity at different laser excitation powers is observed and thus a color can be tuned. The photoluminescence lifetime of green band at 548 nm ($^4S_{3/2}$ level) has been found to be ~446 μs.

1. Introduction

There is growing interest in the development of new full color emitting phosphor materials that combine thermal and chemical stability in air with high emission quantum yield at room-temperature. In order to fulfill the corresponding requirements in various application fields, many research papers on developing new up-conversion materials systems have been reported. Recently, research on rare earth ions doped up-conversion luminescence materials has received considerable attention because of the optical properties arising from the intra 4f transitions. Luminescent properties of lanthanides make them useful for applications in flat-panel display, solid-state laser, optics, optical telecommunication, temperature sensor, as light emitting diodes and *in vitro* and *in vivo* applications.[1–9] Among others, special attention has been given to rare-earth doped hosts emitting in the visible range upon infrared excitation through up-conversion process.[10–15] Co-doping with Yb^{3+} as sensitizer further increases the efficiency of the up-conversion process in rare earths through donor–acceptor processes like Tm^{3+}, Ho^{3+}, Er^{3+} ions.[16–19] Combined Er^{3+}/Yb^{3+} doped low phonon energy host matrices are of special interest, wherein the up-conversion process results in efficient blue, green and red emissions.[20–22] The large spectral overlap between Yb^{3+} emission ($^2F_{5/2} \rightarrow {}^2F_{7/2}$) and Er^{3+} absorption ($^4I_{15/2} \rightarrow {}^4I_{11/2}$) is responsible for such efficient resonant energy transfer (ET) from Yb^{3+} to Er^{3+}.

Among the up-conversion phosphor materials, pyrochlore titanate $Y_2Ti_2O_7$ (YTO) has attracted attention due to its thermal stability, low phonon energy (~712 cm^{-1}), photocatalytic behaviour and high refractive index value (~2.34).[23–27] The optical band gap of host material $Y_2Ti_2O_7$ is ~3.7 eV. This wide band gap of the host reduces a quenching effect on the emission of Ln^{3+} ion. The Ln^{3+} ion doped phosphor gives colors in the blue, green and red regions. In particular co-doping effects on Ln^{3+} emission is critically dependent on the structure of the host matrix, excited state absorption (ESA) and energy transfer (ET) between the f–f transitions of Er^{3+} and/or Er^{3+}/Yb^{3+} combined system. Particularly owing to advances in IR sources, the up-conversion process green-red phosphors are of special interest. Therefore, systematic research on the synthesis mechanism, structure and resultant effects on phosphor characteristics is necessary and worthy of pursuit. Among the solution based synthesis methods the conventional solid-state reaction method is one of the most versatile and low cost techniques to prepare up-conversion phosphor materials. The major drawback in this method is that it is not easy to control the particle size and morphology at higher sintering temperatures.[28] However, the

[a] *Department of Applied Physics, Indian Institute of Technology (BHU), Varanasi, 221005, India. E-mail: psingh.app@itbhu.ac.in; Fax: +91-542-2368428; Tel: +91-542-6701916*

[b] *Department of Physics, Banaras Hindu University, Varanasi, 221005, India. E-mail: kareemskpa@hotmail.com, sbrai49@yahoo.co.in; Fax: +91-542-2368390, +91-542-2368390; Tel: +91-542-2307308, +91-542-2307308*

[c] *King Abdullah Institute for Nanotechnology, King Saud University, Riyadh, 11451, Saudi Arabia*

† Electronic supplementary information (ESI) available: Variation of CIE coordinates with excitation power and comparison of 524 and 661 nm emission bands after normalizing the emission intensity at 548 nm. See DOI: 10.1039/c2cp44195k

sample prepared at higher temperature (~1200 °C) for long duration (~12 h) shows strong photoluminescence because of the fewer number of quenchers on the surface of the particles, which is due to the possibility of reduced dangling bonds on the particle surface. Recently, this problem in nanomaterials was reduced by annealing the as prepared sample at a higher temeperature.[29a] Recently, Cheetham and his co-workers prepared Yb^{3+}, Er^{3+} and Tm^{3+} co-doped Y_2BaZnO_5 phosphors at ~1200 °C and sintered them for several days. Samples show strong green, red, blue and white emission depending on the proportion of the rare earth ions.

It is interesting to see that these samples are excited at very low power (~25–90 mW mm^{-2}).[29b,c] Moreover, the preparation method of colloidal/hybrid nanoparticles by pulsed laser ablation (PLA) with lanthanide ion doped inorganic phosphor as the target is useful in various applications. Amans and his co-workers prepared nanoparticles using laser ablation (having a laser pulse energy between ~2–70 mJ) of doped oxides such as Eu:Y_2O_3, Eu:Gd_2O_3 and Ce:YAG in aqueous solution of 2-[2-(2-methoxyethoxy)ethoxy]acetic acid (MEEAA). The size and number of particles is controlled by varying laser pulse energy and solvent.[30a] Moreover, Er^{3+}/Yb^{3+} co-doped up-conversion materials have great ability to improve solar cell efficiency. The enhancement of solar cell efficiency using up- and down-conversion Ln^{3+} has been reported.[29c,30b,c]

Herein, we have prepared a $Y_2Ti_2O_7$ (YTO) and $Er_xYb_yY_{2-x-y}Ti_2O_7$ (EYYTO) system through the conventional solid state route and studied structural and optical properties of EYYTO. In particular, we illustrate an interesting approach to understand the mechanism of energy transfer from EYYTO (sensitizer) host to the dopants (activator) by incorporating the rare-earth ions (Er^{3+}, Yb^{3+}) which have unique charge-transfer associated excited states in their host (YTO or EYYTO) matrices. Laser power dependence on up-conversion luminescence has been explained through an energy transfer mechanism between the absorbing host and the rare-earth emitters. Further, we have prepared a monodispersed colloidal solution of EYYTO employing laser ablation method and studied its emission and absorption spectra.

2. Experimental

2.1 Synthesis

$Y_2Ti_2O_7$ (YTO) and $Er_xYb_yY_{2-x-y}Ti_2O_7$ (x = 1 and y = 2 at%) (EYYTO) samples were prepared by the conventional solid state route. The starting materials used in the synthesis process were Y_2O_3 (99.99%, Alfa Aessar), TiO_2 (99.9%, Alfa Aessar), Yb_2O_3 (99.98%, Alfa Aessar) and Er_2O_3 (99.9%, Alfa Aessar). For typical synthesis of $Er_xYb_yY_{2-x-y}$ Ti_2O_7 (x = 1 and y = 2 at%) phosphor, the stoichometric composition of these were mixed in a ball mill agate mortar at the speed of 50 rpm for three hours using acetone as a mixing medium. This mixed system was transferred into an alumina crucible and heated to 1200 °C in ambient atmosphere at the rate of 2 °C min^{-1} for 6 h. This was allowed to cool at room temperature by natural processes. The mixture was ground using pestle mortar for 1 h; and pellets of 10 mm in diameter and 2 mm in thickness were prepared. The pellets were sintered at 1300 °C for 12 h. A similar process was used to prepare YTO sample. These samples were used further for the structural and optical characterizations.

2.2 Preparation of colloidal nanoparticles

Colloidal solution of the EYYTO powder was prepared *via* a liquid pulsed laser ablation method. The pellet of the EYYTO powder was immersed in the distilled water medium and the laser light with wavelength 355 nm (with pulse repetition rate 10 Hz, pulse width 6 ns and pulse energy ~80 m J) was incident on the pellet. The laser beam was focused by a convergent lens with 15 cm focal length. The pellet was immersed in water nearly 5 mm underneath the air-water interface. The pellet was rotated and the spot size of the laser beam at the target surface was varied as ~1–2 mm in diameter by adjusting the distance between focusing lens and target of the sample during the process of ablation.

2.3 Characterization

X-ray diffraction (XRD) pattern was measured with a Rigaku miniflex-II diffractometer using CuK_α radiation (1.5404 Å) at 30 kV and 15 mA in the range $10 \leq 2\theta/^\circ \leq 90^\circ$ with a step size of $\Delta 2\theta = 0.02^\circ$. Fourier transform infrared (FTIR) spectrum of the sample was recorded using Shimazu spectrophotometer in the range from 600–400 cm^{-1}. The small amount of sample was mixed with KBr (Sigma Aldrich, 99.99%) in 1 : 5 ratios and a transparent pellet was prepared. The Raman spectra of the YTO and EYYTO were measured with Renishaw micro-Raman spectrometer attached with 514.5 nm Ar^+ laser as an excitation source. The photoluminescence (PL) spectra were recorded using iHR320 (Horiba Jobin Yvon) spectrometer equipped with R928P photon counting photomultiplier tube and a 976 nm diode laser with 2.4 W maximum power as an excitation source. The PL decay measurement for $^4S_{3/2} \rightarrow {}^4I_{15/2}$ transitions of Er^{3+} ion at 548 nm band was carried out with ~976 nm diode source. The luminescence signal was interfaced to a 150 MHz digital oscilloscope (model no. HM 1507, Hameg Instruments). The decay time was determined using the method of non-linear square fit. The goodness of fit was judged on the basis of R^2 value with method of non-linear square fit. The absorption spectrum of the sample was recorded by UV-Vis Perkin Elmer Lambda-35 spectrophotometer. The microstructure analysis was carried out by transmission electron microscope (TEM) employing JEOL operated at an accelerated voltage of 200 kV. A 355 nm radiation (third harmonic) from a pulsed Nd–YAG laser (Spitlight 600, Innolas, Germany) was used to prepare the colloidal solution nanoparticles.

3. Results and discussion

3.1 Structural analysis

3.1.1 XRD study. Fig. 1 shows the XRD patterns of YTO and EYYTO samples along with corresponding (*hkl*) planes. All the peaks are well matched with JCPDS card no. 42-0413. It clearly shows that samples are well crystalline with a face centered

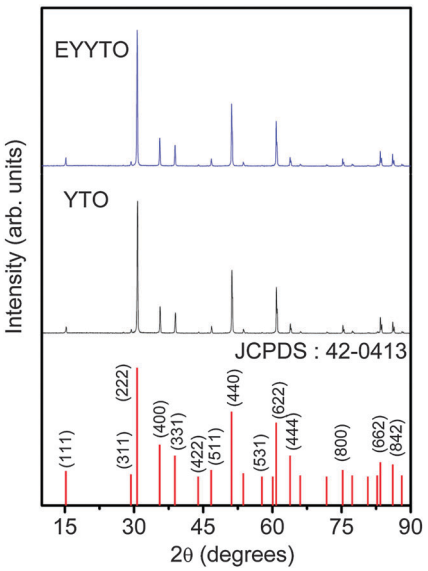

Fig. 1 XRD patterns of $Y_2Ti_2O_7$ (YTO) and Er^{3+}/Yb^{3+} doped $Y_2Ti_2O_7$ (EYYTO) phosphor.

cubic lattice structure.[31] The average crystallite size of the sample were calculated using Scherrer's formula,[32a,b]

$$D = \frac{k\lambda}{\beta_{hkl}\cos(\theta)}$$

where $k = 0.89$, D average crystallite size, λ wavelength of CuK_α, θ Bragg's diffraction angle of the planes and β_{hkl} the corrected full width at half maximum (FWHM). For β_{hkl} correction, β_{inist} (FWHM due to instrument) is removed using Si standard. The average crystallite size of YTO and EYYTO samples were found to be ~87 and 85 nm, respectively. The structure refinement of the samples was carried out using *FullProf* software.[33] The peak profiles were modelled using Pseudo-Voigt function and background was described in terms of a six coefficient polynomial. The R_{wp} (weighted-pattern factor) and S (goodness-of-fit) parameters were used as numerical criterion of the quality of fit of calculated to experimental diffraction data. Fig. 2(a) and (b) show the Rietveld refinement of powder diffraction data of YTO and EYYTO samples. The Bragg reflections, difference in observed and calculated intensity are also shown in the figure itself. The fitting parameters obtained after refinement are listed in Table 1. It was found that the unit cell volume slightly decreased after Er^{3+}/Yb^{3+} doping in YTO. This may be due to small ionic radius of Er^{3+}/Yb^{3+} ions as compared to Y^{3+} ion.[34] The diffraction patterns intensity of EYYTO was found to be slightly less than YTO samples which may be due to defects created in Er^{3+}/Yb^{3+}doped YTO. Inset in Fig. 2(a) shows the expansion of typical Rietveld fitting to the experimental data of (222) plane between 30.4 to 31.1° and the three dimensional polyhedral representation of EYYTO sample is shown in inset of Fig. 2(b). In $Y_2Ti_2O_7$ pyrochlore, the larger cations sit at site A (16*c*) with 8 coordination number while the smaller one sits at site B (6*d*) with 6 coordination. The oxygen atoms occupy the three different crystallographic axes as 48*f*(O_1), 8*a*(O_2) and 8*b*(O_2).

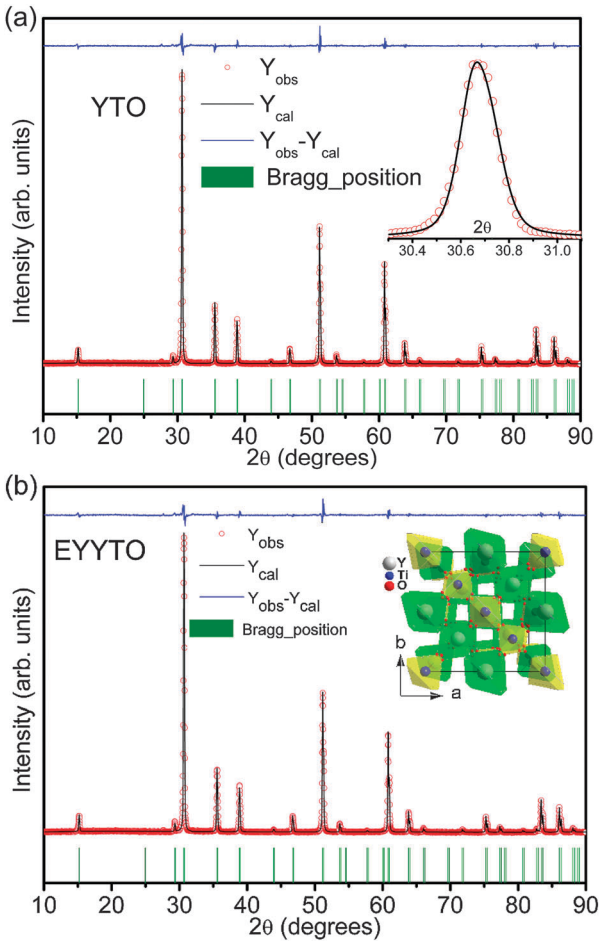

Fig. 2 Rietveld refinements for X-ray diffraction data of (a) $Y_2Ti_2O_7$ (YTO) and (b) 1 at% Er^{3+} and 2 at% Yb^{3+} doped $Y_2Ti_2O_7$ (EYYTO). Calculated positions of Bragg reflections are shown by vertical tick marks (bottom) and top row shows the difference in observed and calculated diffraction peak intensity. Inset of (a) shows the expansion of typical fitting to experimental data between 30.4 to 31.1°. Inset of (b) shows the polyhedral representation of $Y_2Ti_2O_7$.

Table 1 Parameters obtained after refinement of observed XRD data

	Composition	
Parameters	$Y_2Ti_2O_7$ (YTO)	$Y_2Ti_2O_7$:Er^{3+}/Yb^{3+} (EYYTO)
Y(x, y, z)	(0.5, 0.5, 0.5)	(0.5, 0.5, 0.5)
Ti(x, y, z)	(0, 0, 0)	(0, 0, 0)
O_1(x, y, z)	(0.324, 0.125, 0.125)	(0.323(4), 0.125, 0.125)
O_2(x, y, z)	(0.375, 0.375, 0.375)	(0.375, 0.375, 0.375)
Angles(α, β, γ)	(90, 90, 90)	(90, 90, 90)
Lattice parameters (a)	10.095	10.095
Unit cell volume Å^3	1028.92	1028.64
χ^2	4.71	3.91
Y–O_1	2.519	2.5124
Y–O_2	2.1857	2.1855
Ti–O_1	1.9342	1.9377
R_{wp}	17.6	16.1
R_P	15.7	15.5

In $Y_2Ti_2O_7$, 48*f*(O_1) site is tetrahedraly coordinated to two Ti and two Y cations while 8*a*(O_2) is linked with four Y cations, respectively. The third anionic site in the unit cell is 8*b*(O_2)

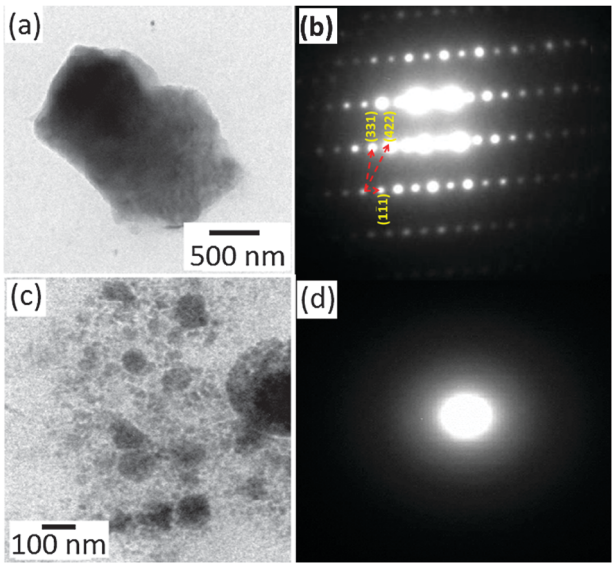

Fig. 3 Transmission electron micrographs of (a) Er^{3+}/Yb^{3+} doped $Y_2Ti_2O_7$ (c) colloidal solution. Their corresponding SAED patterns are shown in (b) and (d), respectively.

which is tetrahedraly coordinated with four Ti cations and generally found to be empty for perfectly ordered pyrochlore.

3.1.2 TEM study. TEM images of EYYTO phosphor and its laser ablated colloidal solution are shown in Fig. 3(a) and (c) along with the corresponding selected area electron diffraction (SAED) patterns in Fig. 3(b) and (d), respectively. An irregular spherical microsphere is observed. The SAED analysis was performed to confirm the crystallinity of the prepared material. The result of SAED patterns reveals corresponding (*hkl*) planes. The average particle size in colloidal solution was found to be ~100 nm.

3.1.3 FTIR study. FTIR spectrum of EYYTO is shown in Fig. 4. The absorption bands appeared at ~417, 436, 484, 494 and 573 cm^{-1} are related to Y–O_1, Y–O_2 and Ti–O, stretching vibrations.[35] The band around 500 and 400 cm^{-1} are assigned to Y–O_1 and Y–O_2 stretching vibrations in the $Y_2Ti_2(O_1)_6O(_2)$

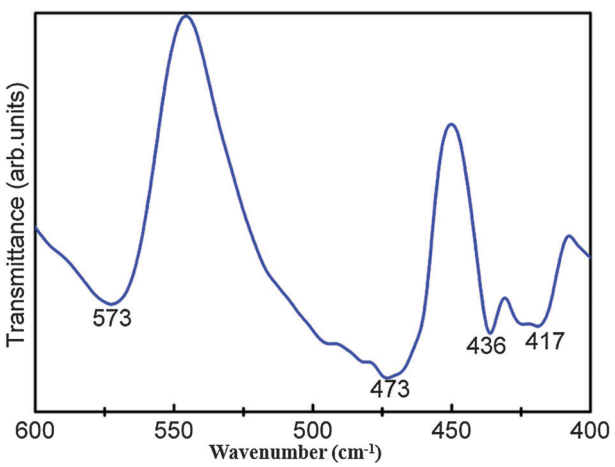

Fig. 4 FTIR spectrum of Er^{3+}/Yb^{3+} doped $Y_2Ti_2O_7$ (EYYTO) phosphor.

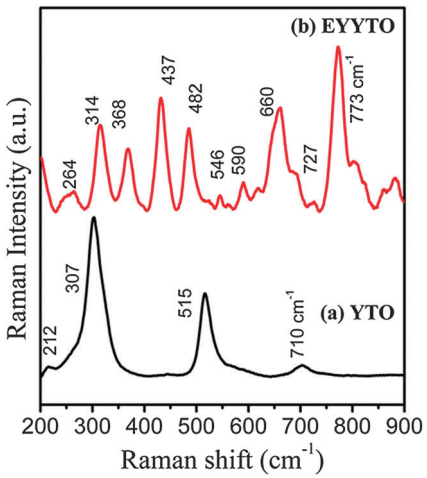

Fig. 5 Raman spectra of (a) YTO and (b) EYYTO samples at room temperature.

polyhedron of $Y_2Ti_2O_7$. Chen *et al.*[36] found the absorption bands of YTO sample at 573, 473 and 417 cm^{-1} which are assigned to Ti–O, Y–O_2 and Y–O_1 stretching vibrations, respectively. These are the main features of the titanate pyrochlore IR-spectra. These vibrations confirm the formation of $Y_2Ti_2O_7$ structure.

3.1.4 Raman study. The Raman spectra of pure YTO and EYYTO samples are shown in the Fig. 5(a) and (b). Since the pyrochlore ($A_2B_2O_7$) is a superstructure of fluorite formed by ordering of A and B cations into uneven crystallographic sites and ordering of anions into three sites 48*f*(O_1), 8*a*(O_2) and 8*b*(O_3). Therefore, Raman spectroscopy provides the degree of disorder in pyrochlore and hence distinguishes between defects pyrochlore to fluorite structures. Raman spectroscopy is more sensitive to metal-oxygen vibrational modes in comparison to metal–metal vibrational modes. There are six Raman active modes found in $A_2B_2O_7$ pyrochlores having space group (*Fd*3*m*, *Z* = 8). These modes arise due to vibration of oxygen at 48*f*(O_1) and 8*a*(O_2). A and B cations do not contribute to active Raman bands because they posses centrosymmetric symmetry with an inversion centre. At room temperature pure YTO shows the well known Raman bands of at ~212, 307, 515, and 710 cm^{-1} and very weak band near 800 cm^{-1}. The active Raman bands in this compound to $\Gamma_{Raman} = A_{1g} + E_g + 4T_{2g}$, the symbols represent the irreducible group representation.[37] Gupta and Brown[38] calculated the active IR and the Raman bands for YTO sample and explained that number of IR and Raman active modes for this system are seven and six, respectively. The active Raman bands were A_{1g}, E_g and $4T_{2g}$ while IR active is $7F_{1u}$. Sanjuan *et al.*[37] explained the characteristic modes of YTO pyrochlore observed at ~310 cm^{-1} which has the contributions from E_g and T_{2g} modes both. The bands at ~515 and 711 cm^{-1} correspond to A_{1g} mode of vibration and one of the T_{2g} mode of vibration, respectively. The A_{1g} frequency mode provides information about the force constant of YTO pyrochlore. The vibration of the TiO_6 octahedra is responsible for the A_{1g} mode of vibration of YTO pyrochlore structure. The major contribution for this mode is mainly due to force constants associated

with O–Ti–O bending.[39] Vanderborre *et al.*[40] explained the Raman spectra of different stannates and titanates for the higher frequency T_{2g} modes of vibrations. These higher T_{2g} modes of vibrations occur due to the force constant of Ti–O bond in TiO_6 octahedra. Recently, Camacho *et al.*[41] studied the Raman spectra of Er^{3+}/Yb^{3+} doped hybrid materials and reported that the band situated near ~368 cm^{-1} is the metal oxygen (Yb–O) similar to the band at 377 cm^{-1} of (Y–O) stretching vibration, while characteristic peaks of Er^{3+} ion are found in the range of ~500–580 cm^{-1} and also some small traces of Raman bands near ~620–680 cm^{-1} and ~780–900 cm^{-1} are observed. Some additional Raman modes with lower intensities are also observed due to local disorder and defects present in the pyrochlore lattice of EYYTO. Radhakrishnan *et al.*[42] described the presence of local disordering and defects in Ca and Mo substituted $Gd_2Ti_2O_7$. They reported that the disordering and defects present in the system distort the translational periodic arrangement of the lattice and hence allows the $k = 0$ selection rule, which is the main cause of the occurrence of additional Raman bands with lower intensities in the EYYTO pyrochlore structure.

3.2 Up-conversion and pump power dependence study

Up-conversion (UC) is a nonlinear optical phenomenon in which light of higher wavelength near infrared or infrared (*i.e.* NIR or IR) is converted into visible or UV (ultraviolet) light through multiphoton absorption and energy transfer (ET) processes.[5] On excitation with 976 nm laser, a large number of bands starting from UV to Vis to NIR could be observed due to Er^{3+} ions. The bands appearing in the green and red regions are very intense and lie in the anti-stoke side of the pump beam. These bands are shown in Fig. 6. In order to understand the UC mechanism involved in the EYYTO system, we have analysed the pump power dependence of up-conversion fluorescence intensity. Emission spectra of EYYTO sample were recorded with ~0.4, 0.7, 0.8 and 1.7 W laser input power in the range of 350–900 nm (Fig. 6). Two prominent bands are observed due to up-conversion at ~524, 548 nm which are responsible for green emission situated in between 500–600 nm with maximum intensity at ~548 nm. These two bands arise due to $^2H_{11/2} \rightarrow {}^4I_{15/2}$, and $^4S_{3/2} \rightarrow {}^4I_{15/2}$ electronic transitions, respectively of the Er^{3+} ion. Also the band observed in the range 600 to 700 nm with maximum intensity at ~661 nm was assigned to the $^4F_{9/2} \rightarrow {}^4I_{15/2}$ transition. Moreover, peaks at ~380, 410 and 487 nm in near UV and blue region of the spectrum with low intensity which is well described in the inset (i) from 380–500 nm. These bands arise due to the electronic transitions namely, from $^4G_{11/2} \rightarrow {}^4I_{15/2}$, $^2H_{9/2} \rightarrow {}^4I_{15/2}$ and $^4F_{5/2} \rightarrow {}^4I_{15/2}$ of Er^{3+} ion on 976 nm excitation. Inset (ii) ranging from 750–900 nm, which are Stark splitting pattern $^4I_{9/2} \rightarrow {}^4I_{15/2}$ of Er^{3+} ion. The Stark splitting clearly demonstrates the highly crystalline nature of EYYTO phosphor. It is also observed that stark splitting of the transition is less in low excitation power and becomes clearer with increasing power. The stark splitting patterns also suggest that Er^{3+} ions are situated in well located crystallite sites of face centered cubic pyrochlore.[15] The levels are populated partially by direct absorption and partly through energy transfer from Yb^{3+} to Er^{3+} ions. Since, Er^{3+} has a poor absorption cross section (1.7×10^{-21} cm^2) than its Yb^{3+} counterpart, which has very high absorption cross section (11.7×10^{-21} cm^2) at 976 nm excitation.[43] Generally, there are two possible processes namely, excited state absorption (ESA) and energy transfer (ET) up-conversion, responsible for up-conversion emission. In the context of ESA processes, the green and red emissions arising from the Er^{3+} ion can be explained on the basis of these two mechanisms, which are result from excitation at 976 nm. The Er^{3+} ion in its ground state absorbs the incident photons and is promoted to $^4I_{11/2}$ excited state, whereas the absorption of the next photons of same energy, Er^{3+} ions is promoted to the $^4F_{7/2}$ level. The ions in $^4F_{7/2}$ level decay through nonradiative channel *via* multi phonon process to $^2H_{11/2}$ and $^4S_{3/2}$ levels. In the ET process, there is probability of two Er^{3+} ions excited to their $^4I_{11/2}$ state *via* GSA or one Er^{3+} ion is promoted in $^4I_{11/2}$ level (GSA) and one Yb^{3+} ion in the $^2F_{5/2}$ level (GSA). The Yb^{3+} ion transfers its energy to Er^{3+} to excite it to $^4I_{11/2}$ level. The two excited Er^{3+} ions in the $^4I_{11/2}$ level exchange their energy and one decays to the ground state $^4I_{15/2}$ and the other is promoted to $^4F_{7/2}$ level. The ion in $^4F_{7/2}$ level, *via* nonradiative relaxation reaches to $^2H_{11/2}$ and $^4S_{3/2}$ levels. The $^2H_{11/2}$ and $^4S_{3/2}$ levels are populated *via* ET and ESA processes. The resulting green emissions at lower levels are due to these $^2H_{11/2} \rightarrow {}^4I_{15/2}$ and $^4S_{3/2} \rightarrow {}^4I_{15/2}$ energy level transitions. The involved transitions of different emitting levels in the up-conversion process *via* ET and ESA along with GSA are schematically shown in the Fig. 8. Also, part of the ion in $^4S_{3/2}$ can further relax and populate the $^4F_{9/2}$ level leading to the $^4F_{9/2} \rightarrow {}^4I_{15/2}$ transition (red emission). The $^4F_{9/2}$ level may also be populated from the $^4I_{13/2}$ level of the Er^{3+} ion by absorption of a 976 nm photon, or by energy transfer from Yb^{3+} ion. The $^4I_{13/2}$ state is initially populated *via* the non-radiative $^4I_{11/2} \rightarrow {}^4I_{13/2}$ relaxation.[44] As the energy gap between the $^4S_{3/2}$ to $^4F_{9/2}$ is quite large (~3000 cm^{-1}), the probability of

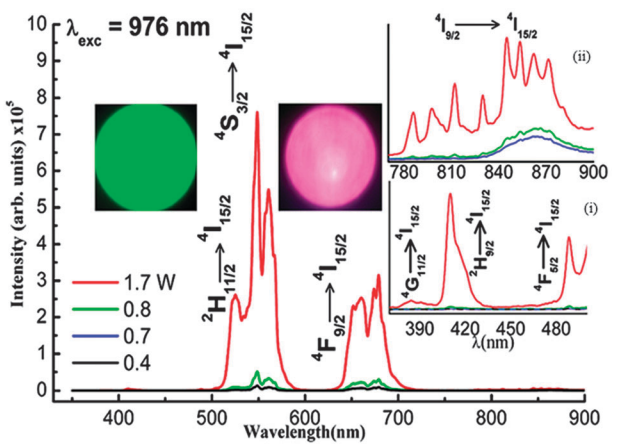

Fig. 6 Emission spectra of Er^{3+}/Yb^{3+} doped $Y_2Ti_2O_7$ phosphor under 976 nm excitation wavelengths at different pump powers (up-conversion). Insets (i) and (ii) show the expansion in 370–440 nm and 775–900 nm. Inset (left) shows the digital photograph of strong green band while the inset (right) shows the red band with the aid of suitable filters.

nonradiative relaxation is smaller while the second channel seems to contribute more effectively. A bright green up-converted light is emitted through $^4S_{3/2} + {}^2H_{11/2} \rightarrow {}^4I_{15/2}$ while a comparatively weak red emission is observed from $^4F_{9/2} \rightarrow {}^4I_{15/2}$ levels.[45,46] The involved mechanism in red band emission is as follows;

$$^2F_{7/2}(Yb^{3+}) \xrightarrow[GSA]{976nm} {}^2F_{5/2}(Yb^{3+})$$

$$^2I_{15/2}(Er^{3+}) \xrightarrow[GSA]{976nm} {}^4I_{11/2}(Er^{3+})$$

$$^4I_{11/2}(Er^{3+}) \rightarrow {}^4I_{13/2}(Er^{3+}) + \text{non-radiative process}$$

$$^2F_{5/2}(Yb^{3+}) + {}^4I_{13/2}(Er^{3+}) \xrightarrow{ET} {}^2F_{7/2}(Yb^{3+}) + {}^4F_{9/2}(Er^{3+})$$

$$^2I_{13/2}(Er^{3+}) + \text{pump photon}$$

$$\xrightarrow{ET} {}^4F_{9/2}(Er^{3+}) \rightarrow {}^4I_{15/2}(Er^{3+}) + \text{red photon}$$

The involvement of two photons is observed for the green (~524 and 548 nm) and red bands (~661 nm) emission, which is well supported by the n value obtained for these bands from Fig. 7(a). Similarly, the up-conversion mechanism channel can be explained for UV and visible bands *i.e.* for ~380, 410 and 487 nm and the involvement of three photons is observed for these bands which is shown in Fig. 7(b). As Er^{3+} and Yb^{3+} ions irradiated with 976 nm radiation and promoted to their excited states (GSA). Since, the absorption cross section of sensitizer (Yb^{3+}) is very much higher in comparison to (Er^{3+}), therefore most photons were absorbed by (Yb^{3+}) ions and transfers its energy to (Er^{3+}) ions *via* ET pathways. The absorption of second photon in excited state promotes the Er^{3+} ions to $^4F_{7/2}$ and $^4S_{3/2}$ levels. A subsequent absorption of third photon promoted the Er^{3+} ion to its $^4G_{7/2}$ levels. To understand the up-conversion influence of the observed luminescence, we have studied the intensity of the band with respect to pump power. The integrated band intensities near UV and visible region in variance with a function of laser excitation power which is shown in the Fig. 7. In the up-conversion mechanism, the emission intensities follow the relation as $I \propto P^n$,[47] where I is the up-conversion intensity, P is the pump power; n is the number of NIR photons involved in the up-conversion. Number of photons n is obtained from slope of the straight line by fitting the bi-logarithmic plot of pump power *versus* emitted intensity. n Values obtained for 524, 548 and 661 nm bands are shown in Fig. 7(a) and the values of n obtained for ~380, 410 and 487 nm as shown in Fig. 7(b) were found to be ~2.83, 3.18 and 3.13, respectively. The slope of the curve at low pump power is linear, which is obvious from region (i) in the figure. As far as moderate power is concerned region (ii) shows quadratic behaviour and for higher pump power marked as region (iii) it shows saturation. Pollnau *et al.*[48] proposed the model on power dependence behaviour of luminescence intensity and explained the slope value for different powers by solving the rate equations and reported that the up-conversion rate enhances for moderate power but for higher values of pump power it becomes almost constant. From the power dependence study, quadratic behaviour is observed for green and red bands while for ultraviolet and blue bands, involvement of three photons was observed. The characteristics emission intensities of green band over red is quite different from those earlier reported. Enhancement in

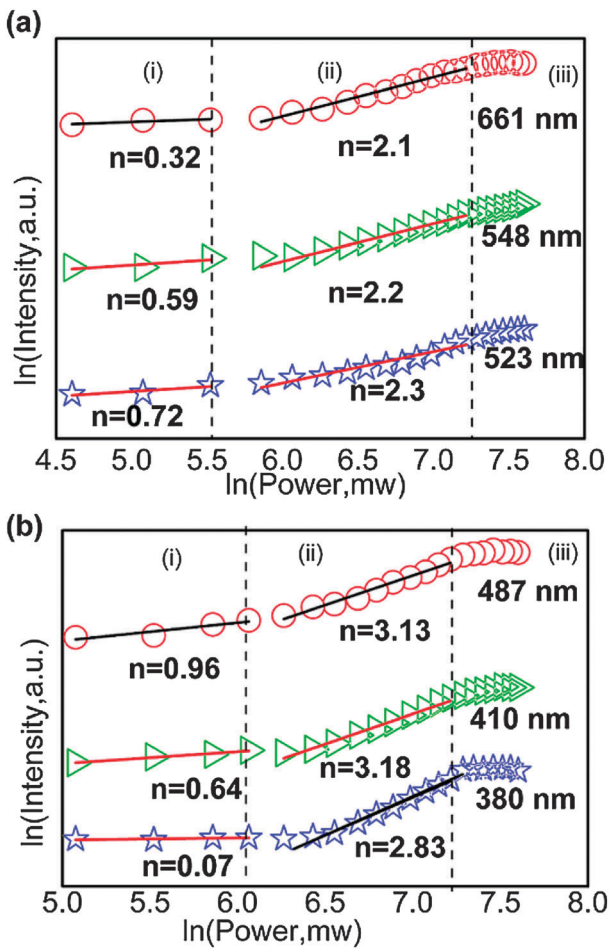

Fig. 7 Power dependence on the up-conversion intensity of (a) bands at 523, 548 and 661 nm and (b) bands at 380, 410 and 487 nm of Er^{3+}/Yb^{3+} doped $Y_2Ti_2O_7$ (EYYTO) phosphor.

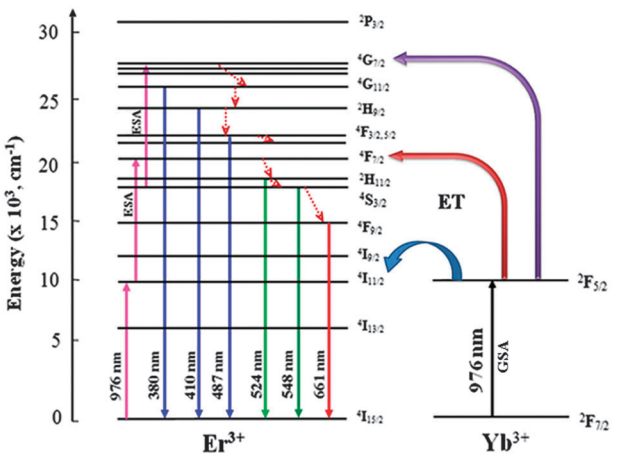

Fig. 8 Energy level diagram of Er^{3+} and Yb^{3+} ions with proposed up-conversion mechanism under 976 nm laser excitation.

photoluminescence intensity was observed even at lower at% of Er^{3+} and Yb^{3+} concentration which demonstrates color tunabilty of the host material. Chen *et al.*[15] has reported the up-conversion behaviour of Er^{3+}/Yb^{3+} doped YTO with varying Yb^{3+} concentration and observed the intense red emission. Recently, photoluminescence modification and energy transfer mechanism was reported by Yan *et al.*[19] for up-conversion behaviour of tri-doped ($Er^{3+}/Yb^{3+}/Tm^{3+}$) $Y_2Ti_2O_7$ inverse opal. It was reported that the improvement in energy transfer occurred between Er^{3+} and Tm^{3+} at 980 nm excitation. Thus the intensity variation observed for the green and red bands is mainly due to energy transfer from (Yb^{3+} to Er^{3+}). The maximum up-conversion intensity is observed for 1 at% Er^{3+} and 2 at% of Yb^{3+} ions. For higher atomic percentage of Er^{3+}, cross relaxation (CR) becomes dominant process and the luminescence quenches.[49]

3.3 Variation of green-red ratio with input diode power

The variation of green to red intensity ratio as a function of excitation power is shown in the Fig. 9. This ratio increases as a function of the excitation power up to ~1.0 W revealing that green emission is dominant over red. As for the higher excitation powers *i.e.* at ~1.2 to 2.4 W, again green emission becomes dominant over the red. In order to understand the variation in the green to red ratio, we normalized the intensity of ~548 nm band and compared its intensity with the intensities of ~524 and 661 nm bands at the same pump power. Detailed analyses of these band intensity variations with input diode powers are given in Fig. S1(a) and (b) (ESI†). For the 524 nm band, the green to red intensity ratio shows an increasing behaviour from low to high power, while for 661 nm band, it is high for low power and decreasing for the high power indicating that green band dominates at higher power. This dominant emission is explained by the proposed model which is given in the inset. The probability of decay rate is not the same for $^4S_{3/2}$ and $^4F_{9/2}$, therefore the excitation power limit is not the same for the both states. In order to explain the observed green and red emissions, let n_1 and n_2 be the no. of photons in the state $^4F_{7/2}$ and $^4F_{9/2}$, respectively. The decay rate $R(p)$ as a function of power from $^4F_{7/2}$ to $^4S_{3/2}$ increases rapidly at the moderate power (up to ~1 W) and $^4S_{3/2}$ state populated and the electronic transition from $^4S_{3/2} \rightarrow {}^4I_{15/2}$, which gives the intense green emission. Since, the phonon vibration energy and heat generated at surface of the sample is enhanced as the power enhances to the higher value and hence the decay probability of photons (say n_2) at $^4S_{3/2}$ to $^4F_{9/2}$ level increases slightly and electronic transition from $^4F_{9/2} \rightarrow {}^4I_{15/2}$, gives slightly improved red emission as clearly seen in the inset. Similar behaviour is reported in the literature for Er^{3+}/Yb^{3+} co-doped SiO_2–Ta_2O_5 glass ceramics by Ferrari *et al.*[44]

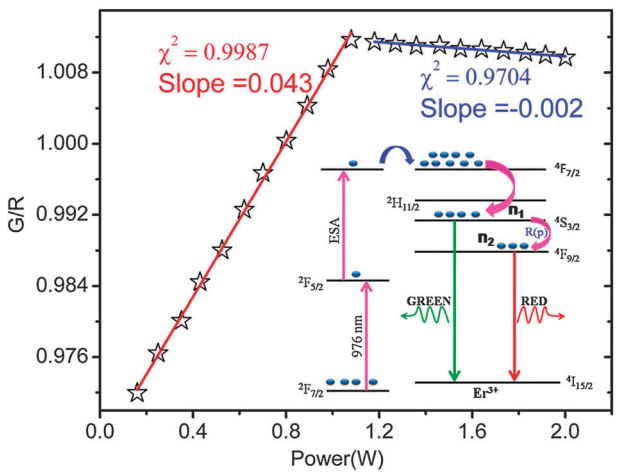

Fig. 9 Variation of intensity of green ($^4S_{3/2} \rightarrow {}^4I_{15/2}$) to red ($^4F_{9/2} \rightarrow {}^4I_{15/2}$) band at different input laser powers of Er^{3+}/Yb^{3+} doped $Y_2Ti_2O_7$ (EYYTO) phosphor. Inset shows the possible transitions for green and red emissions.

3.4. Colloidal solution study

The emission and absorption spectra of the colloidal solution are shown in Fig. 10(a) and (b), respectively. The red emission bands show a very different intensity distribution under 976 nm excitation. In emission spectrum, red band shows variation in intensity distribution in comparison to green. This explains why the excited ions relax rapidly to the lower excited level in colloidal solution. The absorption spectrum of the

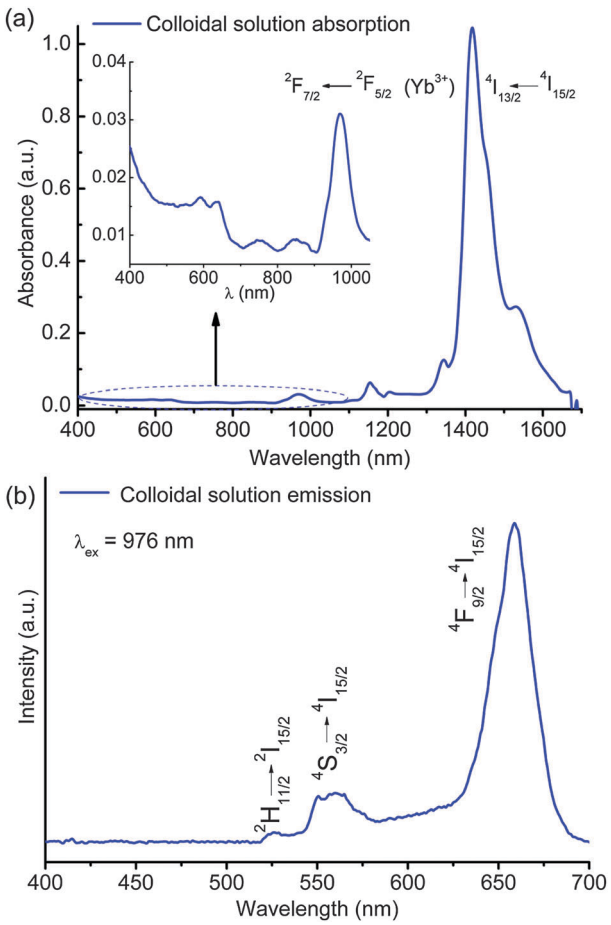

Fig. 10 (a) Absorption spectrum (b) up-conversion spectrum of Er^{3+}/Yb^{3+} doped $Y_2Ti_2O_7$ (EYYTO) colloidal nanoparticles.

colloidal solution is prepared by laser ablation method and shows a strong absorption band at ~1440 nm of Er^{3+} ion due to its $^4I_{15/2} \rightarrow {}^4I_{13/2}$ transition in Er^{3+}. Due to limitations with our instrumental facilities in NIR region, we have been unable to record the emission spectra over the NIR range. A strong emission band from the colloidal solution is observed at 1.5 μm. It is also reported by Liu *et al.*[50] for Er^{3+}/Yb^{3+} doped $NaYF_4$ nanocubes under 976 nm laser diode excitation and found the highest optical amplification gain for 1.5 μm. The strong emission band occurs due to the efficient energy transfer from Yb^{3+} to Er^{3+} ion to give $^4I_{13/2} \rightarrow {}^4I_{15/2}$ transition. Though the absorption band due to Yb^{3+} has a higher absorption cross section than its Er^{3+} ion, its band at ~976 nm appears with weak intensity. The emission band at ~661 nm in Er^{3+}appears with large intensity on excitation with 976 nm radiation. It seems that Er^{3+} ions in $^4I_{13/2}$ level absorb at 976 nm and populate $^4F_{9/2}$ to give $^4F_{9/2} \rightarrow {}^4I_{15/2}$ transition emitting red photon.

3.5 Chromaticity of Er^{3+}/Yb^{3+}:$Y_2Ti_2O_7$ and color tuning

The CIE (*Commission Internationale de l'Eclairage*) system gives the parameters *x* and *y* to demonstrate the color perception. This includes the hue and saturation on a two dimensional chromaticity diagram. Color perception changes from low input diode pump power *i.e.* from ~0.3 W to green to high power 2.4 W to give orangish-red, which is demonstrated in terms of the CIE coordinates, calculated at different powers. It was found that the color coordinates vary with pump power. Since up-conversion efficiency of rare earth doped YTO for different colors depends on excitation power. From Fig. 11 it is obvious that for low input power at ~0.3 W, the color coordinates *x*, *y* are (0.37, 0.57) and for high input power (at ~2.4 W), they are (0.33, 0.65). The variation of CIE coordinates with different input diode powers are given in the Fig. S2 (ESI†) and Table S1(ESI†), respectively.

3.6 Luminescence decay study

The lifetime decay profile of EYYTO sample was recorded under 976 nm (λ_{exc}) excitation by monitoring the emission of green band at ~548 nm ($^4S_{3/2} \rightarrow {}^4I_{15/2}$), is shown in Fig. 12. It is defined as time duration in which the population of higher energy level states is reduced by 1/e of its initial population associated with involved transitions from higher energy to the lower energy state. The measured decay curves were fitted to the equation as $I(t) = I_0 e^{(-t/\tau)}$, where τ is the life time of emitting level. The decay data is found to fit well with mono-exponential fitting having goodness of fit $R^2 = 0.9968$. The calculated value of life time of $^4S_{3/2}$ level is found to be ~446 μs, which is slightly lower than the value reported by Ting *et al.*[27] for Er^{3+} doped YTO. The shorter life value is attributed to the occurrence of energy transfer from $Yb^{3+} \rightarrow Er^{3+}$ and the proposed energy transfer processes are quite reasonable for the EYYTO sample.

In last few years several results have been reported for different Er^{3+} or Er^{3+}/Yb^{3+} co-doped systems widely studied through up-conversion processes (*i.e.*, $BaTiO_3$, TiO_2, Y_2O_3 *etc.*).[51,52] YTO shows comparable phonon frequency to the other hosts like $BaTiO_3$, TiO_2 and Y_2O_3 has a higher thermal and mechanical stability, higher refractive index and wider band gap which opens up its broad and multifunctional applicability. Crystallinity appears in Er^{3+} doped TiO_2 and $BaTiO_3$ samples at ~500 and 700 °C annealing temperature, respectively. Reports show the presence of antase and rutile phases for Er^{3+} doped TiO_2 host between 500–1000 °C annealing temperatures. Optimum up-conversion emission intensity is found at around ~800 °C for TiO_2 host and increases with annealing temperature in $BaTiO_3$. Recently luminescence properties of Eu^{3+} doped $Y_2Ti_2O_7$ have been reported *via* solvothermal process, particles show amorphous nature up to ~750 °C annealing temperature.[53] The present EYYTO phosphor shows tunable up-conversion emission and high crystallinity. This material can be used extensively used for opto-electronic device applications. Also less effort is made to prepare colloidal solution of EYYTO phosphor sample. This solution can

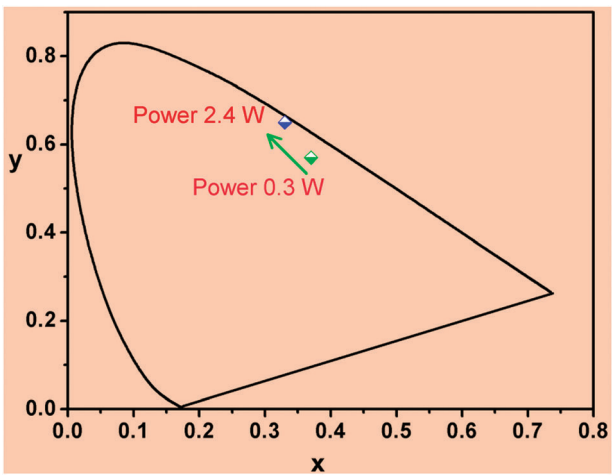

Fig. 11 CIE chromaticity diagram at different laser input power showing color tunabilty of Er^{3+}/Yb^{3+} doped $Y_2Ti_2O_7$ (EYYTO) phosphor.

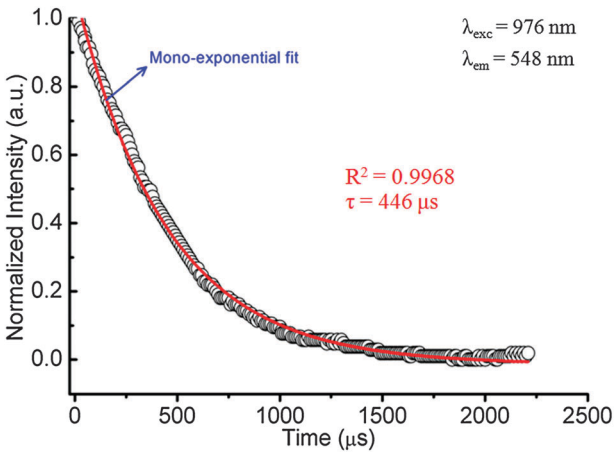

Fig. 12 Luminescence decay curve of Er^{3+}/Yb^{3+} doped $Y_2Ti_2O_7$ (EYYTO) phosphor (λ_{em} = 548 nm, λ_{exc} = 976 nm).

be easily dispersed in polymer thin films and it can be coated on solar cell device for enhancing the solar cell efficiency. The colloidal solution will be further prepared at different excitation powers and are studied for their toxicity and cytotoxicity in forthcoming years.

4. Conclusions

Er^{3+}/Yb^{3+} co-doped yttrium titannate nanophosphors were prepared using solid state reaction route and their comparative structural and up-conversion properties were characterized. Strong green and red emission transitions were observed at ~524, 548 and 661 nm which originated from electronic transitions ($^2H_{11/2} \rightarrow {}^4I_{15/2}$, $^4S_{3/2} \rightarrow {}^4I_{15/2}$ and $^4F_{9/2} \rightarrow {}^4I_{15/2}$) of Er^{3+}, respectively. Power dependence studies of these bands, infer that they arise through a two photon absorption process. The PL properties of Er^{3+}/Yb^{3+} doped samples prepared *via* laser ablation method shows the dominance of red band over green band. It also shows a strong absorption band near 1.45 μm, which will be useful for possible laser materials in optical communication systems. The CIE coordinate varies with input laser power which dictates the color tunabilty of the material. Photoluminescence decay of green band at ~548 nm is studied and found to be mono-exponential in nature. The slightly smaller life time value of $^4S_{3/2}$ is attributed to energy transfer from $Yb^{3+} \rightarrow Er^{3+}$ and inhomogeneity present in the Er^{3+}/Yb^{3+} doped YTO host.

Acknowledgements

Authors (BPS, AKP and RKS) acknowledge financial support from University Grant Commission (UGC) in the form of a fellowship. Authors acknowledge Dr Ranjan K. Singh, Dept. of Physics, BHU, Varanasi, for providing the micro-Raman facility and Dr R. S. Ningthoujam (BARC) for valuable discussions.

References

1 K. Zheng, D. Zhang, D. Zhao, N. Liu, F. Shi and W. Quin, *Phys. Chem. Chem. Phys.*, 2010, **12**, 7620.
2 A. K. Parchur, A. I. Prasad, A. A. Ansari, S. B. Rai and R. S. Ningthoujam, *Dalton Trans.*, 2012, **41**, 11032.
3 A. K. Parchur, R. S. Ningthoujam, S. B. Rai, G. S. Okram, R. A. Singh, M. Tyagi, S. C. Gadkari, R. Tewari and R. K. Vatsa, *Dalton Trans.*, 2011, **40**, 7595.
4 G. S. R. Raju, E. Pavitra, Y. H. Ko and J. S. Yu, *J. Mater. Chem.*, 2012, **22**, 15562.
5 F. Auzel, *Chem. Rev.*, 2004, **104**, 139.
6 F. Wang and X. G. Liu, *Chem. Soc. Rev.*, 2009, **38**, 976.
7 H. A. Hoppe, *Angew. Chem., Int. Ed.*, 2009, **48**, 3572.
8 G. Y. Chen, H. J. Liang, H. C. Liu, G. Somesfalean and Z. G. Zhang, *J. Appl. Phys.*, 2009, **105**, 114315.
9 H. Wang, T. B. Huff, D. A. Zweifel, W. He, P. S. Low, A. Wei and J. X. Chen, *Proc. Natl. Acad. Sci. U. S. A.*, 2005, **102**, 15752.
10 A. Patra, C. S. Friend, R. Kapoor and P. N. Prasad, *J. Phys. B: At., Mol. Opt. Phys.*, 2002, **106**, 1909.
11 G. S. Yi and G. M. Chow, *J. Mater. Chem.*, 2005, **15**, 4460.
12 G. Y. Chen, H. C. Liu, H. J. Liang, G. Somesfalean and Z. Zhang, *J. Phys. Chem. C*, 2008, **112**, 12030.
13 L. W. Yang, Y. Y. Zhang, J. J. Li, Y. Li, J. X. Zhong and P. K. Chu, *Nanoscale*, 2010, **2**, 2805.
14 C. G. Liu, Z. Wang, H. X. Jia and Z. P. Li, *Chem. Commun.*, 2001, 4661.
15 Z. Chen, W. Gong, T. Chen, S. Li, D. Wang and Q. Wang, *Mater. Lett.*, 2012, **68**, 137.
16 J. H. Chung, J. H. Ryu, S. W. Mhin, K. M. Kim and K. B. Shim, *J. Mater. Chem.*, 2012, **22**, 3997.
17 Y. Li, J. Zhang, Y. Luo, X. Zhang, Z. Hao and X. Wang, *J. Mater. Chem.*, 2011, **21**, 2895.
18 X. Quin, T. Yokomori and Y. Ju, *Appl. Phys. Lett.*, 2007, **90**, 073104.
19 D. Yan, J. Zhu, H. Wu, Z. Yang, J. Qiu, Z. Song, X. Yu, Y. Yang, D. Zhou, Z. Yin and R. Wang, *J. Mater. Chem.*, 2012, **22**, 18558.
20 A. Patra, C. S. Friend, R. Kapoor and P. N. Prasad, *Appl. Phys. Lett.*, 2003, **83**, 284.
21 D. Matsuura, *Appl. Phys. Lett.*, 2002, **81**, 4526.
22 S. I. Kink, G. A. Hebbink, L. Grave, F. C. J. M. van Veggel, D. N. R. Reinhoudt, L. H. Loof, A. Polman and J. W. Hofstraat, *J. Appl. Phys.*, 1999, **86**, 1181.
23 P. P. Dai, X. T. Zhang, M. Zhou, X. G. Li, J. K. Yang, P. P. Sun, C. S. Xu and Y. Liu, *J. Am. Ceram. Soc.*, 2012, **95**, 658.
24 A. F. Fuentes, K. Boulahya, M. Maczka, J. Hanuza and U. Amador, *Solid State Sci.*, 2005, **7**, 343.
25 R. Abe, M. Higashi, K. Sayama, Y. Abe and H. Sugihara, *J. Phys. Chem. B*, 2006, **110**, 2219.
26 K. Ariga, A. Vinu, Y. Yamauchi, Q. Ji and J. P. Hill, *Bull. Chem. Soc. Jpn.*, 2012, **85**, 1.
27 C. C. Ting, Y. S. Chiu, C. W. Chang and L. C. Chuang, *J. Solid State Chem.*, 2011, **184**, 563.
28 Z. Pan, Y.-Y. Lu and F. Liu, *Nat. Mater.*, 2012, **11**, 58.
29 (*a*) A. K. Parchur and R. S. Ningthoujam, *RSC Adv.*, 2012, **2**, 10859; (*b*) I. Etchart, M. Berard, M. Laroche, A. Huignard, I. Hernandez, W. P. Gillin, R. J. Curry and A. K. Cheetham, *Chem. Commun.*, 2011, **47**, 6263; (*c*) I. Etchart, A. Huignard, M. Berard, M. N. Nordin, I. Hernandez, R. J. Curry, W. P. Gillin and A. K. Cheetham, *J. Mater. Chem.*, 2010, **20**, 3989.
30 (*a*) D. Amans, C. Malaterre, M. Diouf, C. Mancini, F. Chaput, G. Ledoux, G. Breton, Y. Guillin, C. Dujardin, K. M. Varlot and P. Perriat, *J. Phys. Chem. C*, 2011, **115**, 5131; (*b*) D. Chen, L. Lei, R. Zhang, A. Yang, J. Xu and Y. Wang, *Chem. Commun.*, 2012, **48**, 10630; (*c*) V. M. van der Ende, L. Arts and A. Meijerink, *Phys. Chem. Chem. Phys.*, 2009, **11**, 11081.
31 L. Brixner, *Inorg. Chem.*, 1964, **3**, 1065.
32 (*a*) B. D. Cullity, *Elements of X-ray Diffraction*, Addision-Wesley, Reading, MA, USA, 1959; (*b*) A. K. Parchur and R. S. Ningthoujam, *Dalton Trans.*, 2011, **40**, 7590.
33 J. Rodriguez–Carvajal, FULLPROF a Rietveld and pattern matching analysis program, Laboratoire Leon Brillouin (CEA–CRNS), Paris France.

34 R. D. Shanon, *Acta Crystallogr., Sect. A: Cryst. Phys., Diffr., Theor. Gen. Crystallogr.*, 1976, **32**, 751.
35 J. K. Gill, O. P. Pandey and K. Singh, *Int. J. Hydrogen Energy*, 2012, **37**, 3857.
36 Z. S. Chen, W. P. Gong, T. F. Chen and S. L. Li, *Bull. Mater. Sci.*, 2011, **34**, 429.
37 M. L. Sanjuan, C. Guglieri, S. D. Moreno, G. Aquilanti, A. F. Fuentes, L. Olivi and J. Chaboy, *Phys. Rev. B: Condens. Matter Mater. Phys.*, 2011, **84**, 104207.
38 H. C. Gupta and S. Brown, *J. Phys. Chem. Solids*, 2003, **64**, 2205.
39 S. Brown, H. C. Gupta, J. A. Alonso and M. J. M. Lope, *J. Raman Spectrosc.*, 2003, **34**, 240.
40 M. T. Vanderborre, E. Husson, J. P. Chatry and D. Michel, *J. Raman Spectrosc.*, 1983, **14**, 63.
41 S. A. Camacho, P. H. B. Aoki, C. J. L. Constantino, R. F. Aroca and A. M. Pires, *J. Alloys Compd.*, 2012, **541**, 365.
42 A. N. Radhakrishnan, P. Prabhakar Rao, K. S. Mary Linsa, M. Deepa and P. Koshy, *Dalton Trans.*, 2011, **40**, 3839.
43 C. Strohhofer and A. Polman, *Opt. Mater.*, 2003, **21**, 705.
44 J. L. Ferrari, K. O. Lima, E. Pecoraro, R. A. S. Ferreira, L. D. Carlos and R. R. Goncalves, *J. Mater. Chem.*, 2012, **22**, 9901.
45 K. U. Kumar, K. Linganna, S. S. Babu, F. Piccinelli, A. Speghini, M. Giarola, G. Mariotto and C. K. Jayasankar, *J. Sc. Adv. Mater.*, 2012, **4**, 584.
46 D. Manzani, J. L. Ferrari, F. C. Polachini, Y. Messaddeq and S. J. L. Ribeiro, *J. Mater. Chem.*, 2012, **22**, 16540.
47 F. Pandozzi, F. Vetrone, J. C. Boyer, R. Naccache, J. A. Capobinaco, A. Speghini and M. Bettinelli, *J. Phys. Chem. B*, 2005, **109**, 17400.
48 M. Pollnau, D. R. Gamelin, S. R. Luthi, H. U. Gudel and M. P. Hehlen, *Phys. Rev. B: Condens. Matter Mater. Phys.*, 2000, **61**, 3337.
49 D. L. Dexter, *J. Chem. Phys.*, 1953, **21**, 836.
50 X. Liu, Y. Chi, G. Dong, E. Wu, Y. Quiao, H. Zeng and J. Qiu, *Opt. Express*, 2009, **17**, 5885.
51 A. S. S. de Camargo, L. A. O. Nunes, J. F. Silva, A. C. M. F. Costa, B. S. Barros, J. E. C. Silva, G. F. de Sa and S. A. Junior, *J. Phys. B: At., Mol. Opt. Phys.*, 2007, **19**, 246209.
52 A. Patra, C. S. Friend, R. Kapoor and P. N. Prasad, *Chem. Mater.*, 2003, **15**, 3650.
53 E. Pavitra, G. S. R. Raju and J. S. Yu, *Phys. Status Solidi RRL*, DOI: 10.1002/pssr 201206484.